Journal of Science and Technology
ISSN: 2456-5660 Volume 8, Issue 05 (May -2023)
www.jst.org.in *DOI:https://doi.org/10.46243/jst.2023.v8.i05.pp22 - 32*

Interception amelioration of Chipless RFID Tags Using Deep Learning Techniques

Athul Thomas1[1] | James Kurian[2]

[1]Department of Electronics, Cochin University of Science and Technology, Kerala – 682022, India,

[2]Department of Electronics, Cochin University of Science and Technology, Kerala – 682022, India

To Cite this Article

Athul Thomas1, James Kurian **, Interception amelioration of Chipless RFID Tags Using Deep Learning Techniques** **"** *Journal of Science and Technology, Vol. 08, Issue 05,-May 2023, pp01-21*

Article Info

Received: 26-03-2023 *Revised: 17-04-2023* *Accepted: 27-04-2023* *Published: 10-05-2023*

Abstract

In this paper, we have proposed data-driven methods to enhance the interrogation and reliability of Chip-less Radio Frequency Identification systems. Six binary combinations of an 8-bit RFID tag are fabricated on a Rogers RT / Duroid ® 5880 substrate with a permittivity of 2.2 and a loss tangent of 0.0009 to create the model dataset. The tag's frequency response encompasses eight identifiable frequency resonances in the 3–10 GHz frequency band. By analyzing the spectral signature of the backscattered chip-less RFID tags at possible reach and orientation, two distinct datasets corresponding to ideal (within the anechoic chamber) and natural environments are prepared. The data sets are trained and evaluated using the SVM, KNN, DT and DNN approaches. A validation accuracy of 97.5% is obtained for the DNN model in actual environmental conditions in the presence of clutter and noises. The DNN model attains an accuracy of 99.5% on the ideal dataset and 97.5% on the actual dataset. The model extracted tag information up to 70cm from the interrogator, which is about a 20% increase in reading range compared to conventional interrogation methods.

KEYWORDS: *anechoic chamber; barcode; chipless rfid; deep Learning; svm.*

I. INTRODUCTION

Radiofrequency identification and sensing technology have received a pervasive response in recent years due to their great promises in the field of manufacturing (Abdullah et al., 2020), agriculture (Sedghy, 2019) and the Internet of Things (IoT) (Mulloni & Donelli, 2020). RFID tags have attracted substantial interest over their predecessor barcodes, owing to features such as long reading range, high data rate, high level of security, readability without Line of Sight and the possibility to read multiple tags simultaneously (Akbari et al., 2015). RFID technology encompasses classical radio frequency identification with chip (Active and Semi passive)) and chipless RFID. Conventional RFID systems follows a technology that has already been developed, optimised, and incorporated , while chipless RFID has recently been adopted primarily to minimize the tag price(Herrojo et al., 2019). As it eliminates the costs involved with silicon IC spall in the circuit, chipless RFID technology is undeniably a significant advancement in overcoming the margins and constraints of traditional RFID systems.

In the open literature, chipless RFID tags with varying information density per surface (DPS) have been reported, such as time domain reflectometry tags (Girbau et al., 2012), spectral signature-based chipless tags (Preradovic et al., 2009), and Amplitude/Phase backscatter modulation-based chipless tags. Frequency-domain tags offer higher coding capacity and are prevalent in the existing literature. They can be either a re-transmission type tag (Nijas et al., 2012) or a backscattered type tag (Nijas et al., 2014). Backscattered chipless RFID tags are composed of multiple resonant elements that scatter the ultra-wideband signal from the interceptor depending on the geometry of the individual components and the dielectric constant of the substrate material. The resultant resonance may be encoded using the Absence / Presence Coding method or the Frequency Shift Coding approach (Mandal et al., 2019).

Figure 1 Block diagram of a basic chipless radio frequency identification (RFID) system.

Even though chip-less RFID tags are gaining popularity in the supply chain sector since they are less expensive than conventional RFIDs, they are still in the prototype stage (Costa et al., 2021). It's challenging to evaluate the RCS generated by the backscattered tag and obtain the encoded information from the faint received signal without a chip. Due to their passive nature, chipless RFID tags have inherent drawbacks, such as limited data encoding capacity, short reading range, and high sensitivity to disruptions and interferences. As a result, accurate extraction of tag information from complex power values necessitates careful calibration, proper Time-Gating, strategic measurement choices (Nikitin & Rao, 2006), and efficient Clutter Suppression methodologies (Fawky, Khaliel, El-Awamry, El-Hadidy, & Kaiser, 2015).

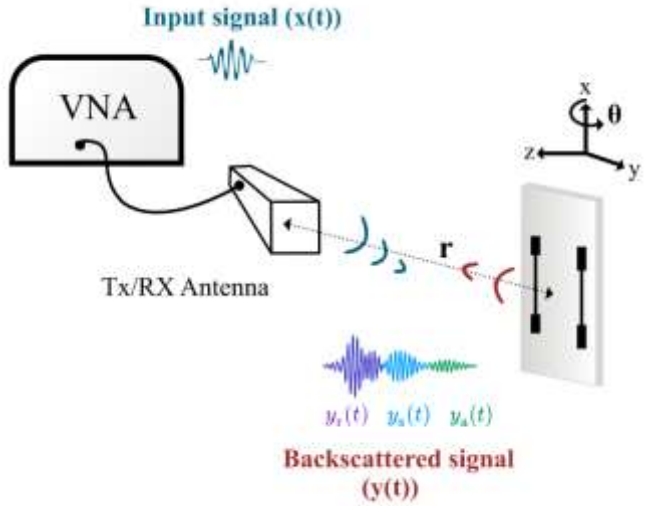

The possibility of an ideal environment may not be available when implementing RFID systems in practice, and conventional signal processing methods often fail to estimate the spectral signature of the tag from background clutter and noises. This paper aims to enhance the reading range and overall reliability of the chipless RFID systems using the state of the art machine learning concepts. Machine learning has made considerable strides in numerous disciplines, from Machine vision systems (Khan & Al-Habsi, 2020) to natural language processing (Klosowski, 2018). Artificial neural networks (ANNs) are computational models that resemble the behaviour of the human nervous system and come in a variety of shapes and sizes depending on their data stream, neuron density, layers, and activation filters such as Feedforward Neural Network, Multilayer Perceptron, Convolutional Neural Network, Recurrent Neural Network, and so on.

In Nijas and Deepak et al., a conventional method followed to design and identify a compact multiple-bit encoded chipless RFID tag using a stepped impedance resonator (SIR) is proposed. The tag utilizes the SIR's fundamental and the first harmonic frequency to represent two-bit information with a single resonator. The suggested RFID tags have an operating range of 50cm in the outdoor environment.

In this article, contemporary neural network models' immense pattern recognition abilities are being exploited to categorize the EM signatures generated by chipless RFID tags. The experiment considered ideal conditions with minimum environment noises and practical scenarios with background clutter and distractions. The response of six proof of concept RFID tags is measured using a vector network analyser in ideal and actual environments at a different distance(r) and orientation (θ). For the study, the tag described in Nijas and Deepak et al. is considered. The dataset prepared is analysed and evaluated using Support Vector Machine (SVM), K-Nearest Neighbor (KNN), Decision Tree (DT) and Deep Neural Network (DNN) models.

II. METHODOLOGY

A. Design Parameters

The analytical approach for determining the SIR's fundamental and harmonic modes of operation is described in Chi-Feng Chen, Ting-Yi Huang, Chi-Ping Chou, and Ruey-Beei Wu, 2006; Kirschning, Jansen, and Koster, 1981; and Sheng-Yuan Lee, 2005. Figure 2 illustrates a typical geometry of the λg/2 type Stepped Impedance Resonator with open and short-circuited extremities and a step transition. Z1 and Z2 denote the Characteristic impedances, and θ1 and θ2 indicate the equivalent electrical length of the SIR elements.

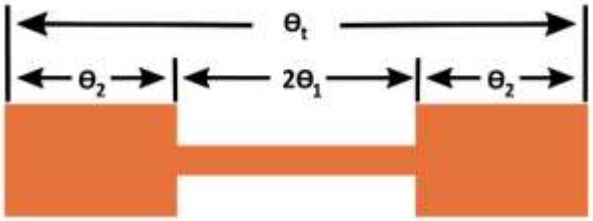

Figure 2 Design parameters of a basic SIR element.

By selecting an appropriate combo of Length Ratio (K) and Impedance ratio (θ), the fundamental frequency (f_0) and subsequent higher order frequencies may be precisely computed. Figure 3 shows the conditions for representing 11, 10 and 01- bit patterns. Λ/2 SIR is required for representing 11- bit configuration, whereas λ/4 with shorted or open end will generate 10 or 01 combinations, respectively. All 28-bit combinations are possible by adequately configuring the SIR elements, as explained. Based on the design parameters explained, tags corresponding to binary combinations of 0 X 44, 0 X 55, 0 X 66, 0 X 77, 0 X 33 and 0 X FF are fabricated on Rogers RT / Duroid ® 5880 substrate with a permittivity of 2.2 and loss tangent of 0.0009 as illustrated in figure 4.

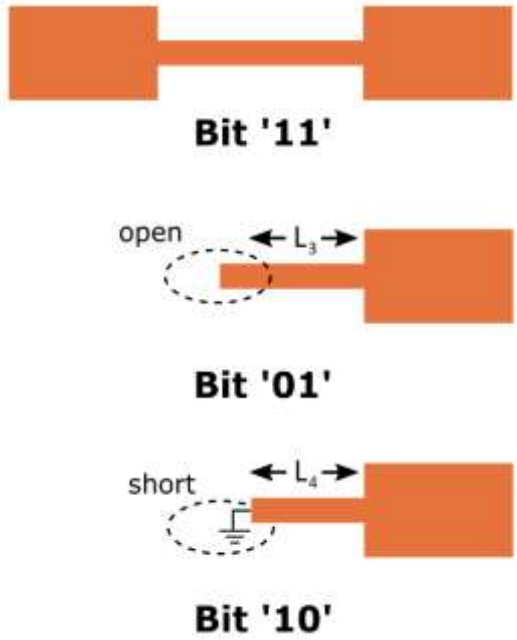

Figure 3 SIR elements for different bit represent- tation a) Bit 11, b) Bit 01, c) Bit 10, where L1, L2, L2' represent the length of individual portions.

Fundamental and first harmonic modes of SIRs, along with Presence or Absence Coding technique is effectively employed in the design and using 4 SIR elements, 8 bit of information is encoded.

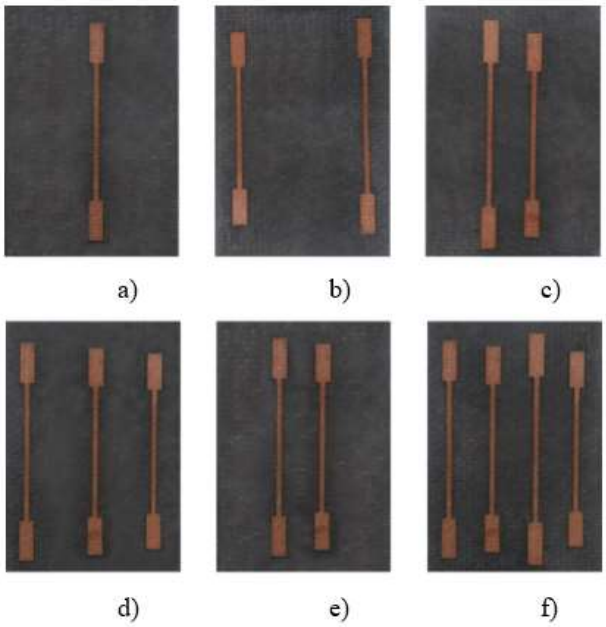

Figure 4 RFID tags fabricated on Rogers RT / Duroid ® 5880 substrate. a) 0X44,b) 0X55,c) 0X66,d) 0X77,e) 0X33,f) 0XFF

B. Measurement

Figure 5 illustrates the measurement setup utilized. The procedures followed in the investigation are depicted in figure 6. The interrogator is a single wideband medium gain horn antenna that transmits Gaussian pulses with frequencies ranging from 3GHz to 10GHz. The source for the measurements is an ROHDE & SCHWARZ ZVB20 Network Analyzer. As shown in the image, the tag under measurement is mounted on an acrylic holder that may be precisely moved or rotated.

Figure 5 Measurement setup utilized in the experiment.

The frequency response of the backscattered chipless RFID tag is determined by adjusting r and θ, where r is the distance of the tag from the interrogator and θ is the orientation angle, as shown in figure 1. A paper box (28cm by 25cm by 5.6cm) is often placed in the vicinity of the tag and the interrogator to replicate the effect of clutter.

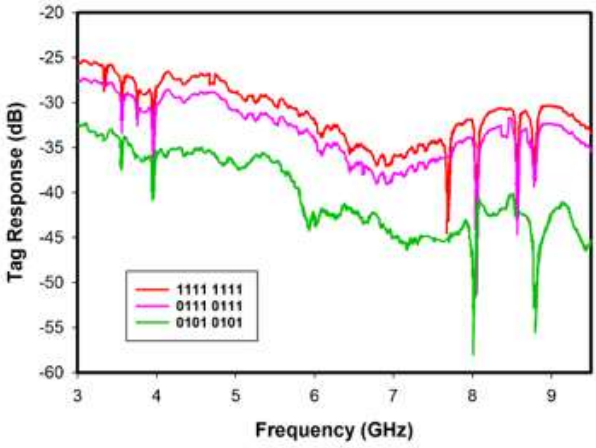

a)

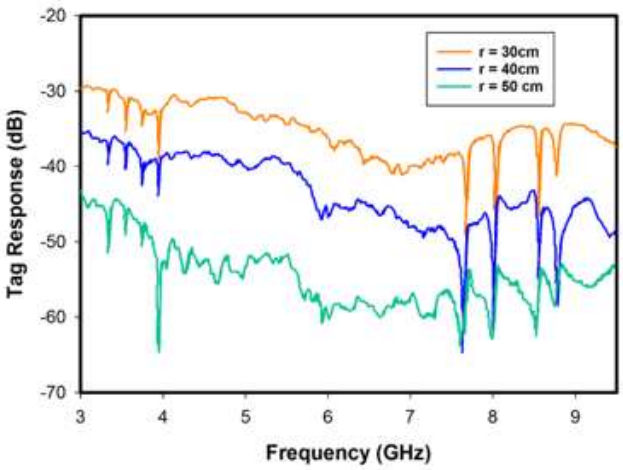

(b)

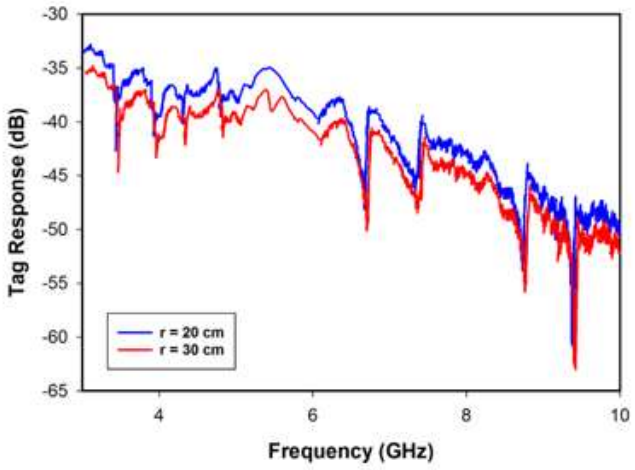

(c)

The experiment addressed both limited and realistic situations, and two independent data sets were created to compare the efficacy of the deep learning model. The first set of data is collected in an ideal setting by conducting the experiments in an anechoic room, as illustrated in figure 5, with microwave-absorbing materials covering the walls, floor, and ceiling. The polyurethane foam impregnated with carbon black ferrite ensures a free space environment by absorbing electromagnetic reflections from surroundings (Fan, 2019). Figure 6a depicts the resonance produced by different RFID tags inside the anechoic chamber. The fluctuation in tag resonance as a function of distance from the horn antenna is shown in figure 6b. The fundamental and harmonic frequencies solely depend on the length of the resonator, and the first harmonic frequency will be equal to twice the fundamental frequency.

The measurements were repeated outside the anechoic laboratory in real-world settings, and a second dataset was also created. Figure 6c shows the response of the tag at two different positions outside the anechoic chamber. From figure 6c, it is clear that in practical situations, the response is disturbed by environmental factors. As the separation between the interrogator and tag increases, the response obtained becomes significantly distorted.

C. Dataset

The Network analyzer was configured with 1001 data points per measurement and bandwidth of 7GHz ranging from 3-10GHz. The Scattering parameter S11 determined will have 1001 distinct reflection values with an interval of 0.007GHz between the 3 to 10GHz frequency span. Six different RFID tag classes are considered corresponding to 0X33, 0X44, 0X55, 0X66, 0X77 and 0XFF hexadecimal combinations.

The first dataset includes a total number of 399 measurements per tag with the following variables; 1) range(r) from 5cm to 30cm in steps of 5cm, 2) range(r) from 30cm to 70cm in steps of 5cm in the presence of clutter (paper box), 3) angle θ from -90° to +90° in steps of 10°. In real-life measurement, external reflections and clutter have a negative impact on the tag resonance, as shown in figure 6c. Also, each observation under the same physical conditions may vary due to measurement errors or ambient changes. A rather more extensive data set is necessary to endure such disturbance and extract the underlying tag signature. Each measurement is repeated roughly three times with more resolution to account for environmental changes and background biasing. The second dataset includes a total number of 777 measures per tag with the following variables; 1) range(r) from 5cm to 30cm in steps of 5cm, 2) range(r) from 30cm to 90cm in steps of 5cm in the presence of clutter (paper box), 3) angle θ from -90° to 90° degree in steps of 5°.

The measured S_{11} parameter is represented as a one-dimensional array (1x1001). The overall size of each dataset is determined by analyzing the training complexity and model performance. The first dataset contains 2394x1001 entries. The second dataset includes 14986x1001 entries. Min-Max scaling is applied to normalize the data that has been mapped from 0-90dB to 0-1. The dataset uses one hot encoding to categorize RFID tags. The diversity of information in the dataset can be further increased by assessing variations in the real/imaginary component of the reflection coefficient or phase variations in the

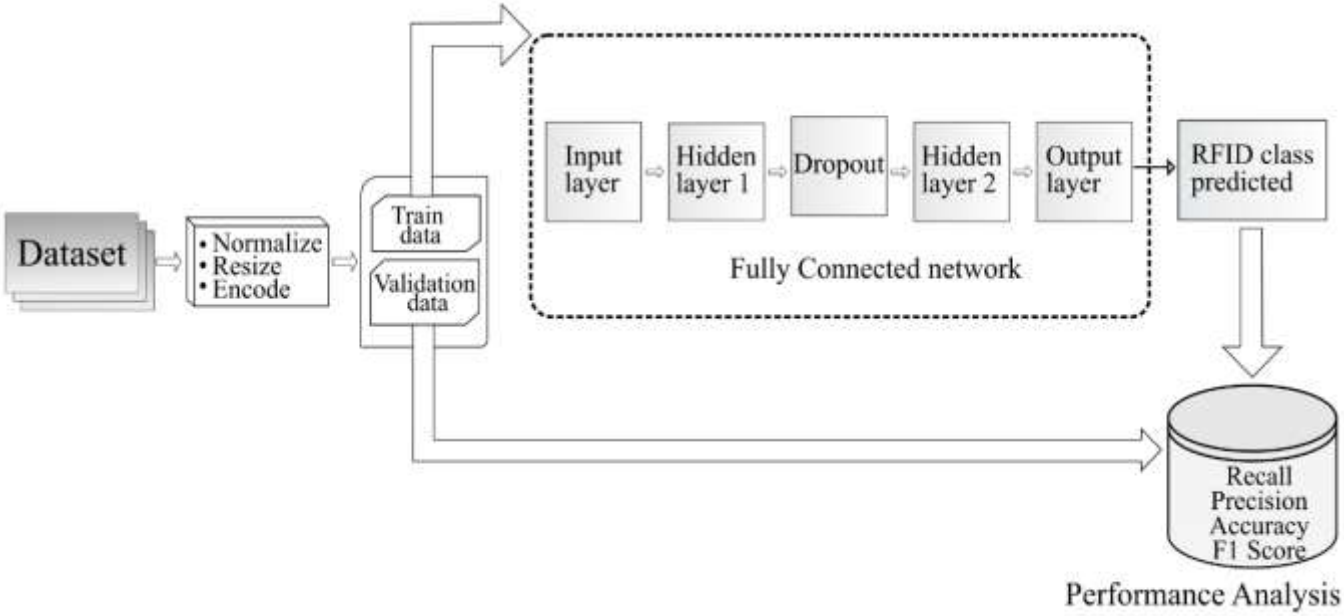

Figure 7 Block diagram of the DNN model

backscattered signal.

D. Deep Learning Methodology

In general, there are two main steps to solving a classification problem with data-driven algorithms: (a) preparing an appropriate dataset in terms of diversity and quality and (b) selecting an efficient machine learning model that results in high prediction accuracy for unseen test samples to support generalizability and avoid biasing. A diverse dataset with enough records considering actual and ideal scenarios is created by interrogating six different RFID tags, as explained in section C. Popular data-driven approaches such as SVM, KNN, DT and DNN were examined on the distribution to identify the best model for classifying RFID tags.

For the classification problems, the objective of the Support Vector Machine model is to determine an appropriate boundary or hyperplanes distinguishing the possible outputs depending on the kernel function specified (Dai & Dong, 2020). KNN is a non-linear learning method that calculates the Euclidean distance between all points near the new information, and the points with the shortest distances are chosen as the best candidates. The decision tree (DT) algorithm is used in the third classifier.

A decision is reached using this non-parametric divide and conquers methodology by traversing a hierarchical graph from a root location to a leaf node (Patel & Prajapati, 2018). Deep neural networks follow a hierarchical learning process which involves a series of non-linear blocks that each converts a depiction at one stage into an illustration at a larger, slightly more abstract level. Complex patterns and relations can be inferred by combining enough of these transitions (LeCun, Bengio, & Hinton, 2015).

Formally, algorithms learn distribution by simplifying weight vectors. The optimization of model parameters based on the distribution will improves the accuracy of the model. The aforementioned models were trained and validated on both the dataset and their accuracy is compared. The DNN model is found to be performing well on the dataset and the details of the model is described below.

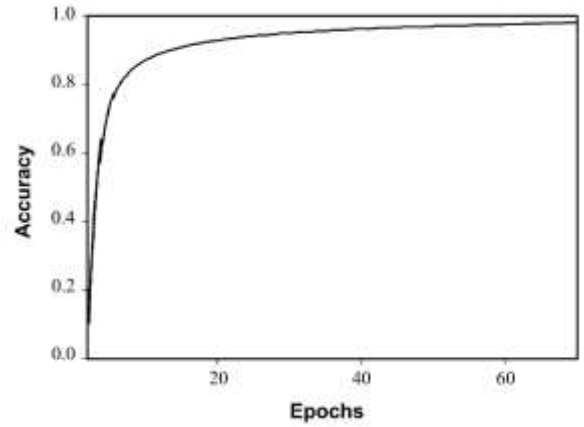

(a)

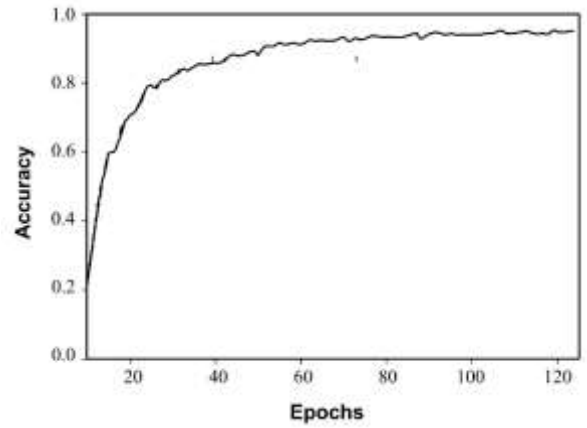

(b)

Figure 8 a) DNN Accuracy plot inside the Anechoic Chamber, b) DNN Accuracy plot outside the Anechoic Chamber

DNN used here features an input layer that accepts flattened S11 parameters, followed by a set of hidden layers and an output layer. The input to the first layer represents the reflection measured at each frequency point as [$S_{11}(f_1)$,S_{11} (f_2).....S_{11} (f_{1001})]. Here, a random search optimization algorithm is used, and the final model diagram is shown in figure 7. Hyperparameter optimization yields an optimal model with an adequate number of hidden units that minimizes the predetermined loss function and hence improves the accuracy on the given distribution. ReLU activation is employed in fully-connected layers considering the computational efficiency, sparsity and reduced likelihood of vanishing gradient. The regularization layer with a dropout rate of 0.25 is introduced to enhance the quality of features by minimizing co-adaptations and over-fitting. The output layer uses Soft-Max as the activation function and has six neurons correlating to the six chipless-ID classes. A 3 fold cross validation was also performed to confirm the performance of the models.

III. RESULTS AND DISCUSSION

As explained in the previous section, the neural network model is evaluated using two independent datasets that address actual and ideal circumstances. The ideal dataset has dimensions of 2394 X 1001, whereas the actual measurement has dimensions of 13986 X 1001. The measurements cover distance r ranging from 5cm to 100cm and angle (θ) from 0 to ±90°. Both the dataset is further divided into a train (80%) and test data (20%).

The model is examined for different ranges of distance and angle combinations to ascertain how far apart from the reader an effective interrogation is possible. The training is carried out for various distances and angles ranging from 40cm-100cm and 40-90° in steps of 10cm/10°, with performance being logged. Figures 8a and 8b show the learning curve representing the validation accuracy over time for the two

datasets. The confusion matrix of both the scenarios is also included in figures 9a and 9b for better illustration.

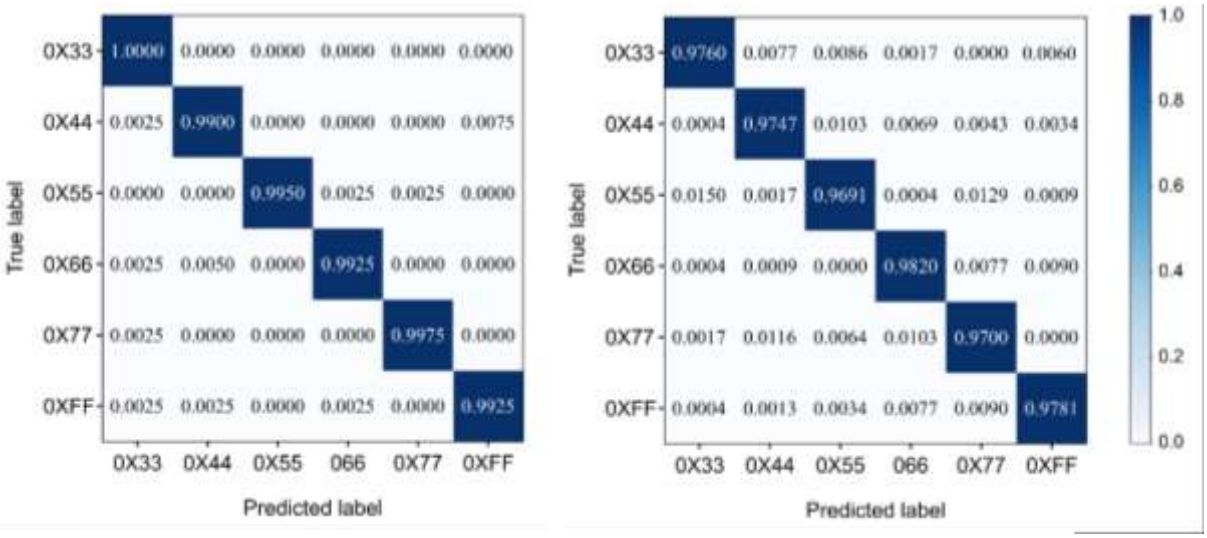

(a) (b)

Figure 9 a) Confusion matrix obtained for ideal dataset b) Confusion matrix obtained for the actual dataset.

With the ideal dataset, the model acquires a validation accuracy of 99.5%, as shown in figure 9a, with minimum model complexity and observations. The model successfully recognized each tag from 5cm to about 70cm covering an angle (θ) of ±65°. When the off-diagonal elements of the confusion matrix shown in figure 9a are examined, it becomes clear that the model doesn't quite mix up among different classes. Figure 10a shows the change in the validation accuracy as the tag is moved or rotated away from the interrogator. As shown in the diagram, the model performs well up to 70cm and 65° from the interrogator with an accuracy of over 99%. Once the tag is moved beyond 70cm or rotated beyond 65°, the accuracy falls abruptly.

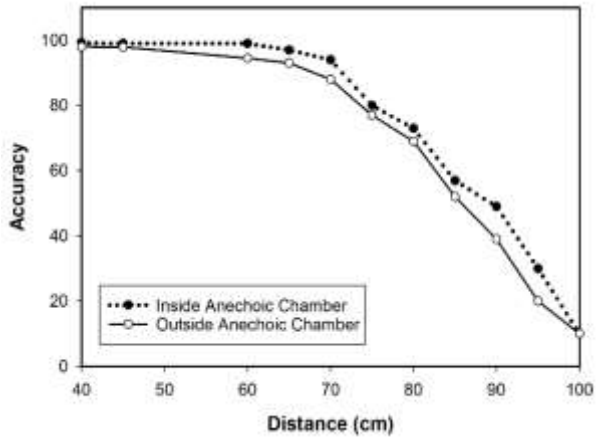

(a)

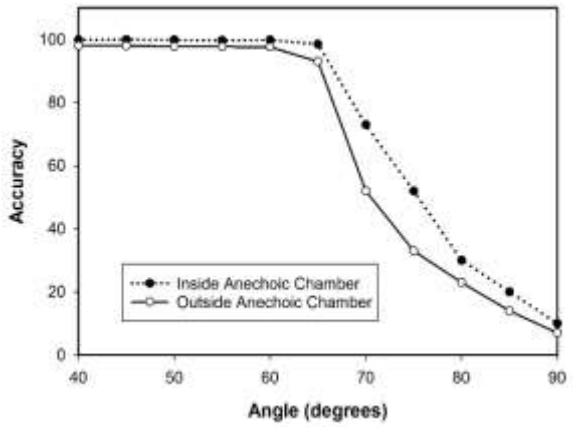

(b)

Figure 10 a) Validation accuracy as a function of r b) Validation accuracy as a function of θ.

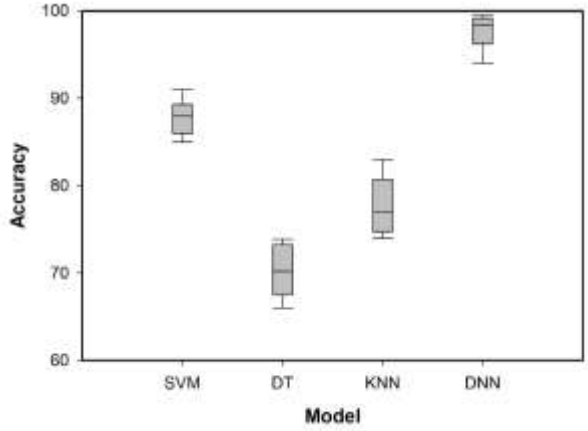

(a)

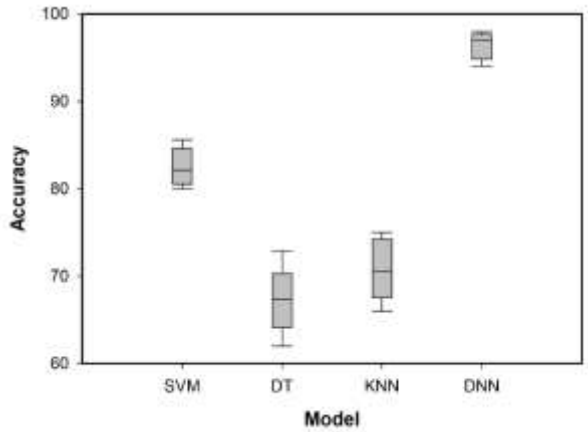

(b)

Figure 11. a) Performance comparison of different models on the ideal dataset b) Performance comparison of different models on the actual dataset

In the second data set, the reflections from the environment and other noises affected the signal received by the interrogator. A diverse dataset is important in avoiding the clutter noises and disturbances affecting the backscattered signal and extracting the tag resonance. As in diagram 8, a complex DNN model with more neurons and hidden layers optimized with a random search optimization algorithm is used.

The model attains a validation accuracy of 97.5%, as shown in figure 8b. The model successfully recognized each tag from 5cm to about 65cm covering an angle of ±65°, as shown in figure 10b. The findings demonstrate that even in real-life situations outside of the anechoic chamber, the DNN model used can extract the signatures of individual RFID Tags.

As per Nijas and Deepak et al., the RFID tag considered in the experiment was successfully measured from 5 cm to 50cm, with an angle θ ±60° inside and outside anechoic conditions. Beyond that, the response

from the interrogator is not visible using conventional methods. However, when deep learning models were used, the interrogator was able to distinguish RFID tags up to 70cm in ideal conditions and up to 65cm in actual conditions with a slight improvement in interrogation angle.

To compare the performance of the DNN model with other machine learning techniques, both datasets are evaluated using SVM, KNN, and Decision Tree approaches. Threefold cross-validation was also performed on all the selected models to corroborate the findings in figure 11. The box plots illustrated in figure11a and 11b show that deep neural network models outperform other machine learning models when optimized appropriately within and outside the anechoic chamber.

IV. CONCLUSION

In this paper, the implementation of data-driven models to enhance the interrogation ability and robustness of chipless RFID systems were demonstrated. The experiments addressed ideal environment conditions within an anechoic chamber and practical scenarios outside the anechoic chamber. The influence of other objects in the interrogation zone and the effect of reader orientation and positions are also examined. Two different datasets are prepared corresponding to the ideal and actual environmental conditions. The measurements are carried out with the following variables; 1) range(r) from 5cm to 100cm in the presence of clutter (paper box), 2) angle θ from -90° to +90°. The datasets prepared are trained and validated using the SVM, KNN, DT and DNN approach. When evaluating the performance of different models, the deep neural network model is found to be achieving better accuracy compared to other models. The DNN model attains an accuracy of 99.5% on the ideal dataset and 97.5% on the actual dataset. The model extracted tag information up to 70cm from the interrogator, which is about a 20% increase in reading range compared to conventional interrogation methods. The method described here is scalable and generalizable to any number of tags or bits with a different environment or noises.

REFERENCES

[1] Abdullah, A., Stroulia, E., & Nawaz, F. (2020). Efficiency Optimization in Supply Chain Using RFID Technology. 2020 IEEE Intl Conf on Dependable, Autonomic and Secure Computing, Intl Conf on Pervasive Intelligence and Computing, Intl Conf on Cloud and Big Data Computing, Intl Conf on Cyber Science and Technology Congress (DASC/PiCom/CBDCom/CyberSciTech), 1–6. https://doi.org/10.1109/DASC-PICom-CBDCom-CyberSciTech49142.2020.00017

[2] Akbari, A., Mirshahi, S., & Hashemipour, M. (2015). Comparison of RFID system and barcode reader for manufacturing processes. 2015 IEEE 28th Canadian Conference on Electrical and Computer Engineering (CCECE), 502–506. https://doi.org/10.1109/CCECE.2015.7129326

[3] Aliasgari, J., & Karmakar, N. C. (2020). Mathematical Model of Chipless RFID Tags for Detection Improvement. IEEE Transactions on Microwave Theory and Techniques, 68(10), 4103–4115. https://doi.org/10.1109/TMTT.2020.2996953

[4] Babaeian, F., & Karmakar, N. C. (2018). Hybrid Chipless RFID Tags- A Pathway to EPC Global Standard. IEEE Access, 6, 67415–67426. https://doi.org/10.1109/ACCESS.2018.2879050

[5] Babaeian, F., & Karmakar, N. C. (2020). Time and Frequency Domains Analysis of Chipless RFID Back-Scattered Tag Reflection. IoT, 1(1), 109–127. https://doi.org/10.3390/iot1010007

[6] Chi-Feng Chen, Ting-Yi Huang, Chi-Ping Chou, & Ruey-Beei Wu. (2006). Microstrip diplexers design with common resonator sections for compact size, but high isolation. IEEE Transactions on Microwave Theory and Techniques, 54(5), 1945–1952. https://doi.org/10.1109/TMTT.2006.873613

[7] Costa, F., Genovesi, S., Borgese, M., Michel, A., Dicandia, F. A., & Manara, G. (2021). A Review of RFID Sensors, the New Frontier of Internet of Things. Sensors, 21(9), 3138. https://doi.org/10.3390/s21093138

[8] Dai, T., & Dong, Y. (2020). Introduction of SVM Related Theory and Its Application Research. 2020 3rd International Conference on Advanced Electronic Materials, Computers and Software Engineering (AEMCSE), 230–233. https://doi.org/10.1109/AEMCSE50948.2020.00056

[9] Fan, D. (2019). Electromagnetic Anechoic Chamber Design and Optimization Method. 2019 International Conference on Microwave and Millimeter Wave Technology (ICMMT), 1–3. https://doi.org/10.1109/ICMMT45702.2019.8992879

[10] Girbau, D., Lazaro, A., & Ramos, A. (2012). Time-coded chipless RFID tags: Design, characterization and application. 2012 IEEE International Conference on RFID-Technologies and Applications (RFID-TA), 12–17. https://doi.org/10.1109/RFID-TA.2012.6404497

[11] Herrojo, Paredes, Mata-Contreras, & Martín. (2019). Chipless-RFID: A Review and Recent Developments. Sensors, 19(15), 3385. https://doi.org/10.3390/s19153385

[12] Khan, A. I., & Al-Habsi, S. (2020). Machine Learning in Computer Vision. Procedia Computer Science, 167, 1444–1451. https://doi.org/10.1016/j.procs.2020.03.355

[13] Kirschning, M., Jansen, R. H., & Koster, N. H. L. (1981). Accurate model for open end effect of microstrip lines. Electronics Letters, 17(3), 123. https://doi.org/10.1049/el:19810088

[14] Mandal, T., Adhikary, M., & Das, S. (2019). FREQUENCY SHIFT ENCODING TECHNIQUE FOR MULTIRESONATOR BASED CHIPLESS RFID TAG. Telecommunications and Radio Engineering, 78(16), 1435–1443. https://doi.org/10.1615/TelecomRadEng.v78.i16.20

[15] Mulloni, V., & Donelli, M. (2020). Chipless RFID Sensors for the Internet of Things: Challenges and Opportunities. Sensors, 20(7), 2135. https://doi.org/10.3390/s20072135
[16] Nastasiu, D., Scripcaru, R., Digulescu, A., Ioana, C., De Amorim, R., Barbot, N., Siragusa, R., Perret, E., & Popescu, F. (2020). A New Method of Secure Authentication Based on Electromagnetic Signatures of Chipless RFID Tags and Machine Learning Approaches. Sensors, 20(21), 6385. https://doi.org/10.3390/s20216385
[17] Nijas, C. M., Deepak, U., Vinesh, P. V., Sujith, R., Mridula, S., Vasudevan, K., & Mohanan, P. (2014). Low-Cost Multiple-Bit Encoded Chipless RFID Tag Using Stepped Impedance Resonator. IEEE Transactions on Antennas and Propagation, 62(9), 4762–4770. https://doi.org/10.1109/TAP.2014.2330586
[18] Nijas, C. M., Dinesh, R., Deepak, U., Rasheed, A., Mridula, S., Vasudevan, K., & Mohanan, P. (2012). Chipless RFID Tag Using Multiple Microstrip Open Stub Resonators. IEEE Transactions on Antennas and Propagation, 60(9), 4429–4432. https://doi.org/10.1109/TAP.2012.2207081
[19] Nikitin, P. V., & Rao, K. V. S. (2006). Theory and measurement of backscattering from RFID tags. IEEE Antennas and Propagation Magazine, 48(6), 212–218. https://doi.org/10.1109/MAP.2006.323323
[20] Patel, H. H., & Prajapati, P. (2018). Study and Analysis of Decision Tree Based Classification Algorithms. International Journal of Computer Sciences and Engineering, 6(10), 74–78. https://doi.org/10.26438/ijcse/v6i10.7478
[21] Preradovic, S., Balbin, I., Karmakar, N. C., & Swiegers, G. F. (2009). Multiresonator-Based Chipless RFID System for Low-Cost Item Tracking. IEEE Transactions on Microwave Theory and Techniques, 57(5), 1411–1419. https://doi.org/10.1109/TMTT.2009.2017323
[22] Rance, O., Perret, E., Siragusa, R., & Lema??tre-Auger, P. (2017). RCS synthesis for chipless RFID: Theory and design. http://search.ebscohost.com/login.aspx?direct=true&scope=site&db=nlebk&db=nlabk&AN=1172384
[23] Sedghy, B. M. (2019). Evolution of Radio Frequency Identification (RFID) in Agricultural Cold Chain Monitoring: A Literature Review. Journal of Agricultural Science, 11(3), 43. https://doi.org/10.5539/jas.v11n3p43
[24] Sheng-Yuan Lee. (2005). Optimum resonant conditions of stepped impedance resonators. 2005 European Microwave Conference, 4 pp. https://doi.org/10.1109/EUMC.2005.1608882